Journal of Structural Biology 177 (2012) 469–476

Contents lists available at SciVerse ScienceDirect

Journal of Structural Biology

journal homepage: www.elsevier.com/locate/yjsbi

Molecular insights into substrate specificity and thermal stability of a bacterial GH5-CBM27 endo-1,4-β-D-mannanase

Camila Ramos dos Santos [a], Joice Helena Paiva [a], Andreia Navarro Meza [a], Junio Cota [b], Thabata Maria Alvarez [b], Roberto Ruller [b], Rolf Alexander Prade [c], Fabio Marcio Squina [b], Mario Tyago Murakami [a,*]

[a] Laboratório Nacional de Biociências (LNBio), Centro Nacional de Pesquisa em Energia e Materiais, Campinas, SP, Brazil
[b] Laboratório Nacional de Ciência e Tecnologia do Bioetanol (CTBE), Centro Nacional de Pesquisa em Energia e Materiais, Campinas, SP, Brazil
[c] Department of Microbiology and Molecular Genetics, Oklahoma State University, Stillwater, OK, USA

ARTICLE INFO

Article history:
Received 9 July 2011
Received in revised form 4 November 2011
Accepted 18 November 2011
Available online 3 December 2011

Keywords:
Mannan endo-1,4-β-mannosidase
Glycoside hydrolase family 5
Carbohydrate binding module 27
Thermotoga petrophila RKU-1
Crystal structure
Substrate recognition

ABSTRACT

The breakdown of β-1,4-mannoside linkages in a variety of mannan-containing polysaccharides is of great importance in industrial processes such as kraft pulp delignification, food processing and production of second-generation biofuels, which puts a premium on studies regarding the prospection and engineering of β-mannanases. In this work, a two-domain β-mannanase from *Thermotoga petrophila* that encompasses a GH5 catalytic domain with a C-terminal CBM27 accessory domain, was functionally and structurally characterized. Kinetic and thermal denaturation experiments showed that the CBM27 domain provided thermo-protection to the catalytic domain, while no contribution on enzymatic activity was observed. The structure of the catalytic domain determined by SIRAS revealed a canonical $(\alpha/\beta)_8$-barrel scaffold surrounded by loops and short helices that form the catalytic interface. Several structurally related ligand molecules interacting with TpMan were solved at high-resolution and resulted in a wide-range representation of the subsites forming the active-site cleft with residues W134, E198, R200, E235, H283 and W284 directly involved in glucose binding.

1. Introduction

Mannan endo-1,4-β-D-mannosidase or 1,4-β-D-mannan mannohydrolase (EC 3.2.1.78), commonly referred as β-mannanase, catalyzes the hydrolysis of β-1,4-mannoside linkages in various mannan-containing polysaccharides, such as glucomannans and galactomannans (Stålbrand et al., 1993; de Vries and Visser, 2001). Degradation of these polysaccharides represents a key step for a number of industrial applications including delignification of kraft pulps (Tenkanen et al., 1997; Montiel et al., 2002), food processing (Sachslehner et al., 2000; Dhavan and Kaur, 2007) and production of second-generation biofuels (Dhavan and Kaur, 2007). In general, these biotechnological processes such as biomass pre-treatments, are performed under extreme environmental conditions regarding pH, osmolarity and temperature. Thus, β-mannanases being stable and functional at high temperatures offer substantial techno-economical advantages.

In addition to their biotechnological relevance, mannan-degrading enzymes also participate in a number of biological processes such as fruit ripening (Pressey, 1989), seed germination (Black, 1996) and remodeling of plant cell walls (reviewed in Schröder et al., 2009). These enzymes have also been used in structural characterization of polysaccharides having β-mannosidic linkages and sequencing of heteropolysaccharides and carbohydrates attached to glycoproteins (Dhavan and Kaur, 2007).

Thermotoga petrophila strain RKU-1 (T) is a hyperthermophilic bacterium isolated from the Kubiki oil reservoir in Niigata (Japan) that grows optimally at 80 °C (Takahata et al., 2001). Some hyperthermostable enzymes produced by this microorganism have demonstrated great potential for industrial applications and served as models for investigating structure–function-stability relationships in multidomain glycosyl hydrolases (Santos et al., 2010, 2011; Squina et al., 2010; Cota et al., 2011).

The β-mannanase from *T. petrophila* RKU-1, TpMan, consists of a CaZy GH5 catalytic core connected to a CBM27 accessory domain by an 100-residue-long linker. To date, only six structures of GH5 endo-β-1,4-mannanases have been solved: *Thermobifida fusca*

Abbreviations: Mannanases: TpMan, from *Thermotoga petrophila*; TfMan, from *Thermobifida fusca*; TrMan, from *Trichoderma reesei*; LeMan, from *Lycopersicon esculentum*; CmMan, from *Cellvibio mixtus*; CjMan, from *Cellvibrio japonicus*; BaMan, from *Bacillus agaradhaerens*; BsMan, from *Bacillus subtilis*; VsMan, from *Vibrio* sp. strain MA-138.

* Corresponding author. Address: Laboratório Nacional de Biociências (LNBio), Centro Nacional de Pesquisa em Energia e Materiais, Rua Giuseppe Maximo Scolfaro, 10000 Campinas, 13083-970 SP, Brazil. Fax: +55 19 3512 1004.
E-mail address: mario.murakami@lnbio.org.br (M.T. Murakami).

1047-8477 © 2011 Elsevier Inc. Open access under the Elsevier OA license.
doi:10.1016/j.jsb.2011.11.021

KW3 (TfMan, PDB codes 1BQC, 2MAN, 3MAN; Hilge et al., 1998), *Trichoderma reesei* (TrMAn, PDB codes 1QNO, P, Q, R, S; Sabini et al., 2000), *Bacillus* sp. JAMB-602 (PDB code: 1WKY; Akita et al., 2004), *Lycopersicon esculentum* (LeMan, PDB code 1RH9; Bourgault et al., 2005), *Bacillus agaradhaerens* (BaMan, PDB code 2WHJ; Tailford et al., 2009), and *Bacillus* sp N16-5 (PDB code: 3JUG; not published). From those, only LeMan and TrMan share some sequence identity (~30%) with TpMan. Both enzymes are non-thermophilic proteins and are poorly related to bacterial β-mannanases because of their low sequence similarity and high degree of glycosylation. Several β-mannanases from both eukaryotic and prokaryotic organisms display high affinity for glucomannans (Pressey, 1989; Tenkanen et al., 1997; Hilge et al., 1998; Tailford et al., 2009; Tanaka et al., 2009); however, the identification of glucose binding sites and their respective mode of interaction remain unknown.

Thus, in order to shed light on the molecular basis of thermal stability and substrate specificity of thermostable bacterial β-mannanases, we performed an extensive biochemical and structural characterization of a β-mannanase from the hyperthermophilic bacterium *T. petrophila* RKU-1. Unfolding studies of deletion mutants demonstrated that the CBM27 accessory domain confers thermo-protection to the catalytic core. The TpMan catalytic core structure was solved by the SIRAS method and several ligand–protein structures were obtained at high resolution revealing the details of the substrate-binding channel and the mechanism of glucose binding.

2. Material and methods

2.1. Cloning, protein expression and purification

The catalytic domain of the endo-1,4-β-D-mannanase (residues 32–393) from *T. petrophila* RKU-1 (TpManΔCT, GenBank Accession Code: YP_001245126) was cloned, expressed and purified according to Santos et al. (2010). Briefly, *Escherichia coli* BL21(DE3)ΔSlyD cells harboring the TpManΔCT/pET-28a vector were grown in selective LB medium to an OD_{600nm} of 0.8 and 0.5 mM IPTG was added to induce heterologous expression for 4 h. The harvested cells were lysed and TpMan isolated from the soluble fraction by nickel-affinity and size-exclusion chromatographies. Sample quality was assessed by polyacrylamide gel electrophoresis under denaturing conditions (Laemmli, 1970) and dynamic light scattering experiments.

Prior to crystallization, the sample was dialyzed against 25 mM Tris–HCl pH 7.5 and concentrated to 12 mg ml^{-1} with Amicon centrifugal ultrafiltration units (Millipore).

2.2. Enzyme assays

Mannan endo-1,4-β-mannosidase activity was determined using a modified 3,5-dinitrosalicylic acid (DNS) method (Miller, 1959). The reaction was performed by mixing 10 μL of the diluted enzyme with 50 μL of mannan or glucomannan at 5 mg/mL for 5 min at 85 °C. The reaction was stopped by the addition of 100 μL DNS reagent followed by boiling the sample in a ~100 °C water bath for 5 min. A response surface methodology was employed to optimize the reaction conditions for TpMan using glucomannan as substrate. The variables pH and temperature were used to design a central composite ($k = 2$) with four central points, totalizing 12 experiments (Table S1) (Myers and Montgomery, 2001; Cota et al., 2011). One unit of mannan endo-1,4-β-mannosidase activity was defined as the amount of enzyme needed to release 1 μmole of mannose equivalents per minute. All experiments were done in triplicate, and average values are reported.

2.3. Capillary zone electrophoresis of oligosaccharides

The oligosaccharide 1,4-β-D-mannohexaose (Megazyme) was derivatized with 8-aminopyreno-1,3,6-trisulfonic acid (APTS) by reductive amination (Chen and Evangelista, 1995). Capillary zone electrophoresis (CZE) was performed on a P/ACE MQD instrument (Beckman Coulter) equipped with laser-induced fluorescence detection. A fused-silica capillary (TSP050375, Polymicro Technologies) of internal diameter of 50 μm and total length of 31 cm was used as separation column for oligosaccharides. Samples were injected by application of 0.5 psi pressure for 0.5 s. Electrophoresis conditions were 15 kV/70–100 μA at a controlled temperature of 20 °C. Oligomers labeled with APTS were excited at 488 nm and emission was collected through a 520 nm band pass filter.

2.4. Circular dichroism spectroscopy

Far-UV CD spectra of the full-length protein (TpMan) and the truncated catalytic domain (TpManΔCT) were measured between 190 and 260 nm in 10 mM phosphate buffer, pH 6.0 at 25 °C with a Jasco J-810 spectropolarimeter (Hachioji City, Tokyo, Japan) using a 2-mm-path-length cuvette and a protein concentration of 0.1 mg/ml. For each experiment, a total of 20 spectra were collected, averaged and corrected by subtraction of a buffer blank and ellipticity was reported as the mean residue molar ellipticity (θ; deg cm^2 $dmol^{-1}$).

In order to investigate the thermal stability, CD spectra were analyzed at different temperatures ranging from 20 to 100 °C. Thermal unfolding was monitored by far-UV CD at 222 nm. The reversibility of thermal denaturation was verified by cooling the denatured sample and subsequent reheating.

2.5. Crystallization, iodine derivatization and data collection

Since attempts to crystallize the intact TpMan were unsuccessful, due to the inherent flexibility of the long linker, crystallization experiments were carried out with a truncated form (TpManΔCT) in which the linker and CBM27 domain were removed.

TpManΔCT crystals were obtained by the sitting drop vapor diffusion method at 293 K by mixing 0.5 μl of protein solution with an equal volume of reservoir solution consisting of 0.1 M citrate pH 5.5, 1 M ammonium phosphate and 0.2 M sodium chloride. The native structure was obtained when a single crystal was directly flash-cooled in a 100 K nitrogen stream without the addition of cryoprotectants. The iodine derivative was prepared according to the quick cryo-soaking method (Dauter et al., 2000) by soaking TpManΔCT crystals in the cryosolution (12.5% (v/v) glycerol) with 0.5 M sodium iodide, for 1 min. Glucose was incorporated by soaking crystals in the reservoir solution containing 0.5 M glucose, for 5 min. Likewise the maltose complex was obtained by adding 0.1 M maltose in the drop solution. The *I*222 crystal form was obtained from a solution containing 0.1 M phosphate pH 4.2, 5% (w/v) PEG-1000, 36% (w/v) ethanol and 10% (v/v) glycerol (Santos et al., 2010).

Diffraction intensities were measured at the tunable-energy MX2 beamline (Brazilian National Synchrotron Light Source, Campinas, Brazil). All datasets were collected with X-ray energy set to 8500 eV except for the derivative crystal whose data were collected at 7797 eV in order to increase the anomalous signal. Data were indexed, integrated and scaled using the HKL2000 package (Otwinowski and Minor, 1997).

2.6. Structure determination and refinement

TpManΔCT structure was determined by single isomorphous replacement anomalous scattering (SIRAS) method using the

native and iodide derivative datasets (Table 1). The positions of thirteen iodine atoms with occupancy over 0.4 were obtained by using the SHELXD program (Schneider and Sheldrick, 2002). The iodine substructure was further used to estimate phases using the SHELXE program, which also employs solvent flattening method to improve the quality of phases (Sheldrick, 2002). Automated model building using the amino acid sequence of TpMan (GenBank code YP_001245126) was performed with the ARP/wARP program (Langer et al., 2008). Around 99% of the molecule was automatically traced. Initial cycles of refinement involved a restrained and overall *B*-factor refinement using the REFMAC5 program (Murshudov et al., 1997). After each cycle of refinement, the model was inspected and manually adjusted to correspond to computed σA-weighted ($2F_o - F_c$) and ($F_o - F_c$) electron density maps using the COOT program (Emsley and Cowtan, 2004). Water molecules were manually added at positive peaks above 3.0 σ in the difference Fourier maps, taking into consideration hydrogen-bonding potential. Crystal structures with resolution better than 1.85 Å resolution were subjected to restrained and anisotropic refinement in later cycles. The *I*222 form and complex structures were solved by molecular-replacement method using the refined native structure as template with the MOLREP program (Vagin and Teplyakov, 1997). Data collection and refinement statistics are summarized in Table 1.

3. Accession Numbers

Coordinates and structure factors have been deposited in the Protein Data Bank with the Accession Codes 3PZG, 3PZ9, 3PZM, 3PZN, 3PZI, 3PZO and 3PZQ.

4. Results and discussion

4.1. Functional characterization

TpMan was incubated with APTS-labeled mannohexaose and cleavage products resolved by capillary zone electrophoresis (Fig. S1). The major cleavage product was mannotriose with detection of minor amounts of mannobiose and mannotetraose, confirming that TpMan is an endo-β-1,4-mannanase.

A Central Composite Design with two variables (pH and temperature) was used to optimize TpMan reaction conditions (Table S1). Both wild-type (WT) and catalytic-domain proteins established maximal activity at the acidic pH range of 4.5–6.5 (Fig. S2). The truncated catalytic domain had optimal activity at a lower temperature range (79–89 °C) when compared to the WT protein (81–93 °C) (Figs. S2B and D). This difference may be an indication that the full-length WT protein is more thermotolerant than the truncated catalytic domain. A similar thermoprotection effect was also observed for Man26 from the thermophilic bacterium *Caldicellulosiruptor* strain Rt8B.4, which contains two tandem N-terminal CBM27s (Roske et al., 2004). The deletion of both accessory domains reduced the optimal temperature for catalysis from 80 to 60 °C (Roske et al., 2004).

4.2. How useful is the CBM27 accessory domain for catalytic function?

A kinetic study was performed with full-length WT and catalytic-domain proteins using 1,4-β-D-mannan and konjac glucomannan as substrates (Table 2). Both TpMan and TpManΔCT had a clear preference for konjac glucomannan, exhibiting a significant higher catalytic efficiency (Table 2). Preference for konjac glucomannan has also been shown for endo-1,4-β-mannosidase from *Aspergillus niger* BK01 (Bien-Cuong et al., 2009), which shares 32% of amino acid sequence identity with TpMan. Moreover, the *A. niger* mannosidase contains no accessory domain indicating that the molecular determinants for glucomannan specificity reside exclusively in the catalytic domain. Indeed, deletion of the CBM27 domain from TpMan had no affect on enzyme specificity (Table 2). In contrast, Man5C from *Vibrio* sp., a GH5 mannanase with a CBM27 accessory domain, showed strong positive interaction of the accessory domain with enzyme kinetics improving catalytic efficiency (k_{cat}/K_m) (Tanaka et al., 2009). On the other hand, Man5C was isolated from a mesophilic bacterium and shares only 37% of amino acid sequence identity with TpMan thus suggesting distinctive roles for the accessory domain.

Unconventionally, the deletion of the accessory domain has no statistically relevant effect on the catalytic efficiency upon both mannan and konjac glucomannan (Table 2). For both substrates, the truncated catalytic domain showed higher V_{max}. In addition, substrate-binding assays showed that TpMan was not adsorbed by insoluble mannan corroborating our kinetic results (results not shown).These data suggest that the accessory domain in TpMan contributes neither to increase catalytic efficiency nor for substrate specificity.

4.3. The CBM27 accessory domain is critical for thermal stability

The apparent minor effect of the CBM27 accessory domain on TpMan enzymatic function as well as the lower temperature optimum of the truncated catalytic domain led us to examine a possible role of CBM27 in enzyme stability. Circular dichroism of full-length WT and truncated catalytic-domain proteins showed typical α/β fold spectra (Fig. 1A), which are in full agreement with crystallographic data. The full-length protein displayed a slighter global residual molar ellipticity when compared to the truncated catalytic domain (Fig. 1A). This effect can be attributed to the built-in unstructured 100-amino acid residue-long linker in the full-length protein (Fig. 3S).

To evaluate the role of CBM27 on enzyme stability, thermal denaturation experiments were performed. As predicted, the deletion of the CBM27 accessory domain reduced the melting temperature from 100 to 88 °C (Fig. 1B), confirming the importance of CBM27 for thermal stability. Thus, based on these biochemical and biophysical evidences, the accessory domain of TpMan should be properly referred as a thermostabilizing domain instead of a carbohydrate-binding module.

4.4. TpMan structure

TpMan shares low amino acid sequence identity with other structurally determined mannanases (~30%). The most similar mannanases are LeMan, TrMan and CmMan (from *Cellvibrio mixtus*, PDB codes 1UUQ and 1UZ4), which present 33%, 33% and 26% of identity and structural superposition rmsd values of 1.6, 1.9 and 2.0 Å, respectively (Fig. 2A, left). CmMan is an exo-cleaving enzyme with only one substrate binding subsite (−1) (Dias et al., 2004). BaMan and TfMan, are endo-cleaving mannanases with a clear ability to cleave glucomannan, but are poorly related to TpMan.

The three-dimensional structure of the TpMan catalytic domain folds into a classical $(\beta/\alpha)_8$ barrel (Fig. 2A). The C-terminal barrel core of β-strands is surrounded by loops and short helices that form a flat molecular surface around the catalytic groove. The active-site cavity has a volume of 1.507 $Å^3$ (Fig. S4A) and is populated by a number of aromatic and acidic amino acids including catalytic residues, E198 and E317 (Figs. S4B and S5). In the TpMan active-site geometry, E198 is hydrogen bonded to H278 and W134 side chains, whereas E317 is coordinated by R71 and Y280 side chains (Fig. S5). Residues Y45, W73, N197, R200, E235, W284 and W350 forming the catalytic interface are absolutely conserved within

Table 1
Data and refinement statistics for TpManΔCT structures.

	Crystalline form I	Crystalline form II	Iodine	Glucose	Maltose	Maltose + Glycerol
Data collection						
Space group	I222	$P2_12_12_1$	$P2_12_12_1$	$P2_12_12_1$	$P2_12_12_1$	$P2_12_12_1$
Cell dimensions						
a, *b*, *c* (Å)	91.03, 89.97, 97.90	55.46, 83.35, 92.18	55.55, 83.63, 92.66	55.43, 83.23, 91.92	55.11, 83.19, 91.52	55.29, 83.30, 92.08
Resolution (Å)	30.00–1.40 (1.45–1.40)*	30.00–1.42 (1.47–1.42)	30.00–1.82 (1.89–1.82)	30.00–1.55 (1.61–1.55)	30.00–1.92 (1.99–1.92)	30.00–1.55 (1.61–1.55)
Mosaicity (°)	0.9	0.3	0.5	0.4	1.0	0.6
R_{sym} (%)	5.1 (33.7)	7.2 (56.8)	9.0 (31.1)	7.3 (52.2)	9.5 (50.9)	7.1 (56.0)
I/σ (I)	40.3 (4.9)	30.2 (2.2)	24.5 (8.9)	23.2 (2.9)	25.0 (5.0)	24.7 (2.4)
Completeness (%)	96.5 (78.7)	98.4 (86.0)	99.3 (98.2)	99.9 (99.1)	99.6 (99.3)	97.7 (84.5)
Unique reflections	76,427 (6160)	80,074 (6891)	39,216 (3790)	62,462 (6068)	32,825 (3225)	61,007 (5208)
Multiplicity	12.1 (8.1)	9.1 (5.3)	13.6 (12.5)	6.1 (5.3)	10.0 (10.5)	7.1 (5.7)
Structure refinement						
R_{work}/R_{free} (%)	15.4/18.4	14.5/17.8	–	14.0/18.3	16.3/21.0	17.1/20.2
Overall B factor	17.4	17.8	–	17.0	18.5	17.4
No. protein atoms	2950	2943	–	2937	2942	2944
No. water molecules	319	417	–	370	265	291
Ligands	TRS–GOL	–	–	GLC	MAL	MAL–GOL
RMSD bond lengths (Å)	0.030	0.030	–	0.027	0.025	0.033
RMSD bond angles (°)	2.301	2.229	–	2.073	1.997	2.639
Ramachandran plot						
Most favored regions (%)	96.9	96.6	–	96.9	96.1	96.9
Allowed regions (%)	3.1	3.4		3.1	3.9	3.1
PDB entry code	3PZG	3PZ9	–	3PZI	3PZO	3PZQ

* Values in parentheses are for highest-resolution shell.

Table 2
Apparent kinetic parameters of TpMan and TpManCT.

	β-1,4-Mannan		Glucomannan (Konjac)	
	TpManΔCT	TpMan	TpManΔCT	TpMan
V_{max} (IU/mg)	250 ± 10	100 ± 5	203 ± 6	114 ± 4
K_m (mg/mL)	1.71 ± 0.16	1.52 ± 0.23	0.80 ± 0.11	1.02 ± 0.19
K_{cat} (s^{-1})	178	126	148	145
K_{cat}/K_m	104	83	165	142

all other β-mannanases with significant amino acid sequence identity (>30%) to TpMan (Fig. 2B).

In order to determine the mechanisms that guide substrate binding interactions of a hyperthermostable β-mannanase, six protein crystals complexed with natural and mimetic oligosaccharides were obtained (Fig. S6). The seven TpMan structures, one native and six carbohydrate complexes shared high overall similarity (RMSD < 0.4 Å); however, local differences were observed in side chain conformations of residues at the protein surface due to distinct crystalline contacts.

4.5. Protein–ligand interactions

Glucose and maltose ligands were incorporated using the soaking method, which yielded high-resolution structures enabling accurate interpretations of binding modes (Fig. S6). The preference for glucomannan as substrate by TpMan (Table 2) motivated the soaking with glucose (GLC) and maltose (MAL) molecules, since structural determinants for glucose binding remain unknown.

In the glucose-TpMan complex crystal, the monosaccharide occupied the +1 subsite and displayed an unexpected orientation in which the reducing O1 atom was pointing to the negative binding subsite (Fig. 3A). This steric positioning was stabilized by several hydrogen bonds with residues E198, R200, E235, H283 and W284.

When TpMan crystals were soaked in the reservoir solution containing 100 mM maltose, three maltose (MAL) molecules were incorporated; one at a remote site participating in crystal packing (Fig. S7A) with no apparent biological relevance and two located at the active-site pocket (Fig. 3B). MAL1 was found at -3 and -2 subsites, and MAL2 was attached to +1 and −1 subsites (Fig. 3B). Both ligands made extensive interactions with the catalytically-relevant residues and aromatic gate-keepers. Analogously to the glucose complex, MAL1 also adopted a pose in which the free O1 atom was turned to the substrate recognition area (Fig. 3B).

Residue N197 is conserved in all GH5 β-mannanases (Sabini et al., 2000) and was found in LeMan structure interacting with the −1 mannosyl group (Bourgault et al., 2005). Mutating this residue to alanine caused loss of activity in *E. chrysanthemi* mannanase (Bortoli-German et al., 1995). In TpMan complexes with glucose and maltose, this residue was not making any contacts with ligands, indicating that N197 is exclusively involved in mannose recognition.

A complex with carbohydrate mimetics including hydroxylated organic compounds, tris and glycerol, were also obtained. They were found at the active-site pocket spanning −3 to +1 subsites and a detailed interaction map is shown in Fig. S7B. The TpMan crystal complex with maltose and glycerol showed a similar configuration observed in the maltose complex with the exception of MAL1, which was replaced by two glycerol molecules (Fig. S7C).

The presence of multiple ligands at the +1 subsite is compatible with the broad substrate specificity exhibited by TpMan, which hydrolyzes glucomannan, mannan and other mannan-containing polysaccharides. The ligand–protein complexes examined in this study revealed a thorough recognition and interaction map of glycosyl groups with residues forming the catalytic interface of TpMan.

4.6. Mapping of substrate-binding subsites

Comparative structural analysis of TpMan complexes with other mannanase complexes permitted us to map the substrate

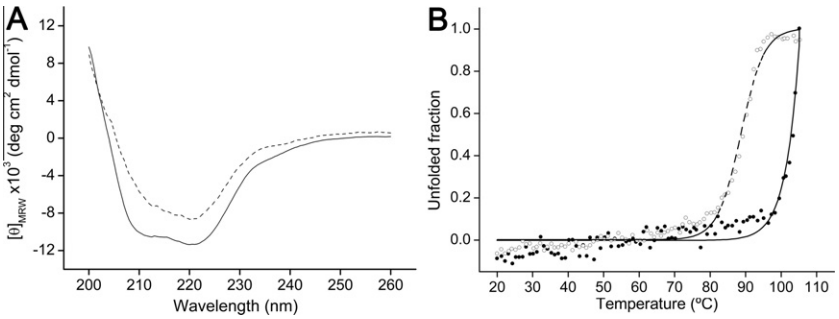

Fig.1. Biophysical characterization of TpMan constructs. (A) Far-UV CD spectra and (B) thermal denaturation of wild-type (continuous line) and ΔCT (dashed line) proteins. Experimental denaturation data are shown as open and full circles for ΔCT and WT constructs, respectively.

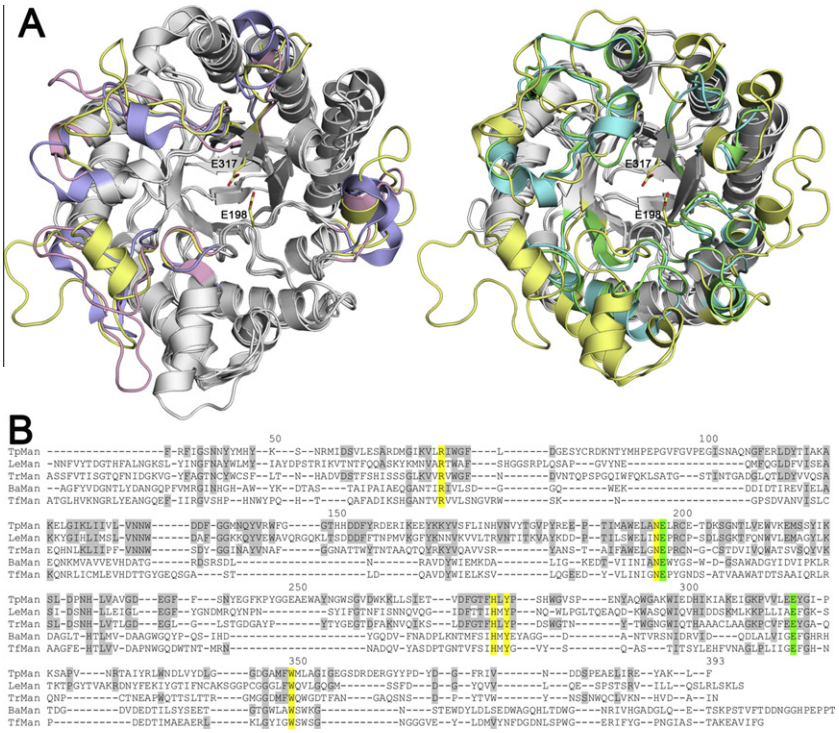

Fig.2. Sequence and structural analysis of TpMan. (A) Structural superposition of TrMan (pink, left), LeMan (blue, left), BaMan (cyan, right), TfMan (green, right) on TpMan (yellow, both). The catalytic residues, E198 and E317, are drawn as sticks with carbon atoms in yellow. (B) Multiple sequence alignment of TpMan with other β-mannanases with known 3-D structures. Residues identical to those of TpMan are shaded in gray. The residues strictly conserved in all β-mannanases and cellulases belonging to GH5 family are highlighted in blue (catalytic residues) and yellow. (For interpretation of the references to colour in this figure legend, the reader is referred to the web version of this article.)

binding subsites (Fig. 4). The ligands found in TpMan structures covered −3, −2, −1 and +1 substrate-binding subsites and the −4 and other positive binding subsites were suggested by structural comparisons.

From the eight residues strictly conserved among GH5 mannanases and cellulases (Hilge et al., 1998), seven are present in TpMan. All conserved residues encompass −1 and +1 subsites including R71, N197, E198, H278, Y280, E317 and W350 (Fig. 4Bi). The -2 subsite formed by residues Y45, W73 and D371 is also conserved in LeMan and TrMan (Fig. 4Bii). However, in the +1 subsite of TpMan, there is a non-conserved histidine residue (H283), which is replaced by a glutamine in LeMan and by a serine in TrMan and with no equivalent residue in both TfMan and BaMan (Fig. 4Bi). In the native structure, H283 displayed a double side-chain conformation (Fig.S8), whereas in the sugar-complex structures, it adopts a defined rotamer conformation in proximity to the aromatic residues W280 and F373 (Fig. S8). In addition, this residue participates in the coordination of MAL and GLC molecules, suggesting a role in substrate recognition and interaction.

The structure of TfMan with a mannotriose bound to the active site (PDB code 3MAN) revealed the residues forming −2, −3 and −4 subsites (Hilge et al., 1998). In this complex structure, a flat surface was observed at the −4 subsite (Fig. S9D), whereas in the TpMan there is a narrow cleft at the equivalent position (Fig. S9A). The residues D84, K85, S359 and D360, which made contacts with the glycosyl residue at the −3 subsite in the TpMan-maltose complex, are closing the aperture and may establish the −4 subsite (Fig. 4Biii). This region is also different in LeMan and TrMan, which contain a wider cleft (Figs. S9B and S9C, respectively), indicating that the −4 subsite in TpMan is unique.

The −3 subsite is also different when compared to other mannanases, mainly because of residue Y370 that makes hydrophobic stacking interactions with the saccharide ring (Fig. 4Biv). This residue is absent in all other mannanases and in the TfMan structure a

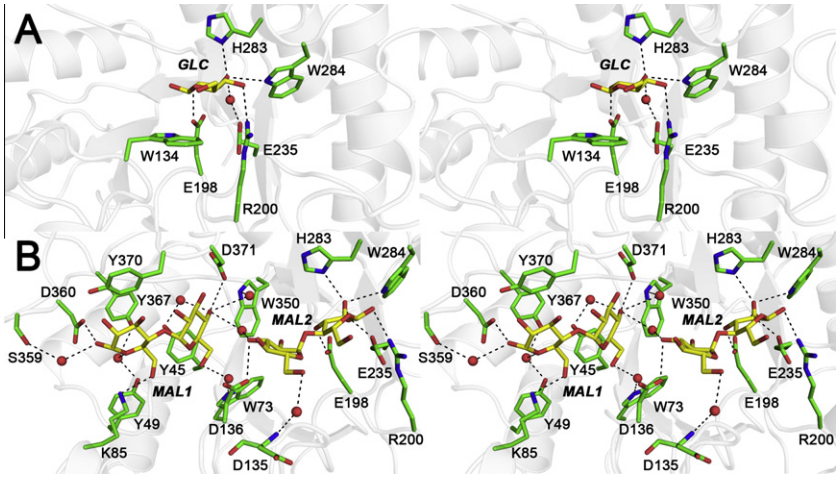

Fig.3. Stereo view of interactions between ligands and active-site residues of TpMan: (A) glucose and (B) maltose complexes.

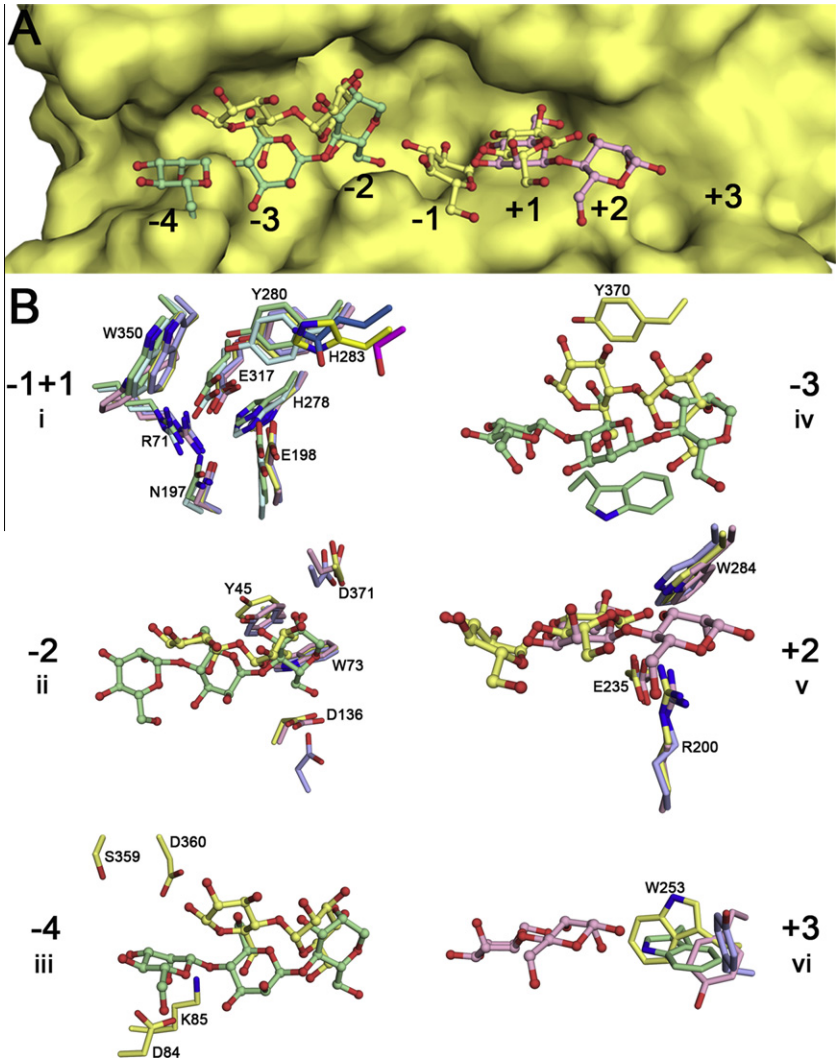

Fig.4. Comparison of TpMan substrate-binding sites with other endo-β-1,4-mannanases. (A) Molecular surface representation of TpMan with substrates bound to the active site. (B) Details of the residues forming the subsites: (i) −1 and +1, (ii) −2, (iii) −4, (iv) −3, (v) +2 and (vi) +3. The carbon atoms of residues and ligands are colored according to each endo-β-1,4-mannannase: TpMan and maltose in yellow, TrMan and mannobiose in pink, TfMan and mannotriose in green, LeMan in blue and BaMan in cyan.

similar role is played by residue W30 (Fig. 4Biv). TpMan has a phenylalanine residue, F137, at the corresponding position, which does not seem to interact with the substrate.

Despite no ligand was observed occupying the +2 subsite in several TpMan structures, residues R200, E235 and W284 located downstream to the +1 subsite are conserved in LeMan and TrMan (Fig. 4Bv). Furthermore, these residues made direct or water-mediated hydrogen bonds with GOL, GLC and MAL molecules that were found at the +1 subsite (Figs. 3 and S7), suggesting that they form the +2 subsite in TpMan.

The +3 subsite was proposed to be formed by residue W171 in TfMan (Hilge et al., 1998) and structural superposition with TpMan indicates that W253 is the equivalent residue (Fig. 4Bvi). In Leman and TrMan, this residue is substituted by a tyrosine, and in BaMan, there is no corresponding residue.

In summary, multiple ligand-complex structures showed that TpMan can bind glycosyl groups at subsites ranging from −3 to +1. In LeMan and TrMan those residues involved in binding of glycosyl groups, comprising subsites −2, −1, +1 and +2, are conserved indicating a similar molecular recognition pattern of gluco-substituted mannans. Studies on BaMan indicated the −2 subsite in determining specificity however, in TpMan, TrMan and LeMan the −2 subsite as well as additional distal subsites are different, suggesting a distinctive structural mechanism.

5. Concluding remarks

The carbohydrate-binding modules have been associated with targeting the parental catalytic domain to the appropriate substrate enhancing the specific activity of the enzyme (Bolam et al., 1998; Boraston et al., 2003; Carrard et al., 2000). Our biochemical data suggested that CBM27 of TpMan is not implicated in substrate selectivity and has no significant effect on enzyme kinetics. On the other hand, the accessory domain confers thermal stability to the catalytic domain, indicating a structural role. Biophysical characterization of other *T. petrophila* glycosyl hydrolases containing CBMs showed similar thermo-protective effects. However, the mechanism by which CBM27, an independent domain connected to the catalytic domain by a 100-residue-long linker, interferes with enzyme stability remains unknown.

The crystal structure of the catalytic domain, solved by the SIRAS method, unveiled the molecular topology of the catalytic interface of TpMan and several ligand-complex structures allowed us to define each subsite forming the large substrate-binding channel and to identify residues relevant for glucomannan recognition. Glucose and maltose complexes revealed that subsites ranging from −3 to +1 are able to bind glycosyl groups so that the saccharide adopts an unusual orientation with the free O1 atom turned to the substrate-binding subsites.

The biochemical and structural dissection of this hyperthermostable GH5-CBM27 endo-1,4-β-mannanase from *T. petrophila* contributes to a better understanding of the molecular determinants for substrate binding, particularly for gluco-substituted mannans and presents an unconventional facet of some carbohydrate-binding modules more related to structural stability instead of enzyme function.

Acknowledgments

This work was supported by grants from the Fundação de Amparo à Pesquisa do Estado de São Paulo to MTM (10/51890-8) and FMS. RAP has funding from the Department of Energy, awards 06103-OKL and ZDJ-7-77608-01. We gratefully acknowledge the provision of time on the facilities MX2 beamline (LNLS), Robolab (LNBio) and LEC (LNBio) at the National Center for Research in Energy and Materials (Campinas, Brazil).

Appendix A. Supplementary data

Supplementary data associated with this article can be found, in the online version, at doi:10.1016/j.jsb.2011.11.021.

References

Akita, M., Takeda, N., Hirasawa, K., Sakai, H., Kawamoto, M., et al., 2004. Crystallization and preliminary X-ray study of alkaline mannanase from an alkaliphilic *Bacillus* isolate. Acta Crystallogr., Sect. D: Biol. Crystallogr. 60, 1490–1492.

Bien-Cuong, D., Thi-Thu, D., Berrin, J.-G., Haltrich, D., Kim-Anh, T., et al., 2009. Cloning, expression in *Pichia pastoris*, and characterization of a thermostable GH5 mannan endo-1,4-β-mannosidase from *Aspergillus niger* BK01. Microb. Cell Factor 8, 59.

Black, M., 1996. Liberating the radicle: a case for softening up. Seed Sci. Res. 6, 39–42.

Bolam, D.N., Ciruela, A., McQueen-Mason, S., Simpson, P., Williamson, M.P., et al., 1998. *Pseudomonas* cellulose-binding domains mediate their effects by increasing enzyme substrate proximity. Biochem. J. 331, 775–781.

Boraston, A.B., Revett, T.J., Boraston, C.M., Nurizzo, D., Davies, G.J., 2003. Structural and thermodynamic dissection of specific mannan recognition by a carbohydrate binding module, TmCBM27. Structure 11, 665–675.

Bortoli-German, I., Haiech, J., Chippaux, M., Barras, F., 1995. Informational suppression to investigate structural functional and evolutionary aspects of the *Erwinia chrysanthemi* cellulase EGZ. J. Mol. Biol. 246, 82–94.

Bourgault, R., Oakley, A.J., Bewley, J.D., Wilce, M.C., 2005. Three-dimensional structure of (1,4)-beta-D-mannan mannanohydrolase from tomato fruit. Protein Sci. 14, 1233–1241.

Carrard, G., Koivula, A., Söderlund, H., Béguin, P., 2000. Cellulose-binding domains promote hydrolysis of different sites on crystalline cellulose. Proc. Natl. Acad. Sci. USA 97, 10342–10347.

Chen, F.T., Evangelista, R.A., 1995. Analysis of mono- and oligosaccharide isomers derivatized with 9-aminopyrene-1,4,6-trisulfonate by capillary electrophoresis with laser-induced fluorescence. Anal. Biochem. 230, 273–280.

Cota, J., Alvarez, T.M., Citadini, A.P., Santos, C.R., Oliveira-Neto, M., et al., 2011. Mode of operation and low resolution structure of a multi-domain and hyperthermophilic endo-β-1,3-glucanase from *Thermotoga petrophila*. Biochem. Biophys. Res. Commun. 406, 590–594.

Dauter, Z., Dauter, M., Rajashankar, K.R., 2000. Novel approach to phasing proteins: derivatization by short cryo-soaking with halides. Acta Crystallogr., Sect. D: Biol. Crystallogr. 56, 232–237.

de Vries, R.P., Visser, J., 2001. Aspergillus enzymes involved in degradation of plant cell wall polysaccharides. Microbiol. Mol. Biol. Rev. 65, 497–522.

Dhavan, S., Kaur, J., 2007. Microbial mannanases: an overview of production and applications. Crit. Rev. Biotechnol. 27, 197–216.

Dias, F.M., Vincent, F., Pell, G., Prates, J.A., Centeno, M.S., et al., 2004. Insights into the molecular determinants of substrate specificity in glycoside hydrolase family 5 revealed by the crystal structure and kinetics of *Cellvibrio mixtus* mannosidase 5A. J. Biol. Chem. 279, 25517–25526.

Emsley, P., Cowtan, K., 2004. Coot: model-building tools for molecular graphics. Acta Crystallogr., Sect. D: Biol. Crystallogr. 60, 2126–2132.

Hilge, M., Gloor, S.M., Rypniewski, W., Sauer, O., Heightman, T.D., et al., 1998. High-resolution native and complex structures of thermostable beta-mannanase from *Thermomonospora fusca* – Substrate specificity in glycosyl hydrolase family 5. Structure 6, 1433–1144.

Laemmli, U.K., 1970. Cleavage of structural proteins during the assembly of the head of bacteriophage T4. Nature 227, 680–685.

Langer, G.G., Cohen, S.X., Perrakis, A., Lamzin, V.S., 2008. Automated macromolecular model building for X-ray crystallography using ARP/wARP version 7. Nat. Protoc. 3, 1171–1179.

Miller, G.L., 1959. Use of dinitrosalicylic acid reagent for determination of reducing sugar. Anal. Chem. 31, 426–428.

Montiel, M.D., Hernández, M., Rodríguez, J., Arias, M.E., 2002. Evaluation of an endo-beta-mannanase produced by *Streptomyces ipomoea* CECT 3341 for the biobleaching of pine kraft pulps. Appl. Microbiol. Biotechnol. 58, 67–72.

Murshudov, G.N., Vagin, A.A., Dodson, E.J., 1997. Refinement of macromolecular structures by the maximum-likelihood method. Acta Crystallogr., Sect. D: Biol. Crystallogr. 53, 240–255.

Myers, R.H., Montgomery, D.C., 2001. Response Surface Methodology, second ed. John Wiley & Sons, New York.

Otwinowski, Z., Minor, W., 1997. Processing of X-ray diffraction data collected in oscillation mode. Methods Enzymol. 276, 307–326.

Pressey, R., 1989. Endo-β-mannanase in tomato fruit. Phytochemistry 28, 3277–3280.

Roske, Y., Sunna, A., Pfeil, W., Heinemann, U., 2004. High-resolution crystal structures of Caldicellulosiruptor strain Rt8B.4 carbohydrate-binding module CBM27-1 and its complex with mannohexaose. J. Mol. Biol. 340, 543–554.

Sabini, E., Schubert, H., Murshudov, G., Wilson, K.S., Siika-Aho, M., et al., 2000. The three-dimensional structure of a *Trichoderma reesei* beta-mannanase from

glycoside hydrolase family 5. Acta Crystallogr., Sect. D: Biol. Crystallogr. 56, 3–13.
Sachslehner, A., Foidl, G., Foidl, N., Gübitz, G., Haltrich, D., 2000. Hydrolysis of isolated coffee mannan and coffee extract by mannanases of *Sclerotium rolfsii*. J. Biotechnol. 80, 127–134.
Santos, C.R., Squina, F.M., Navarro, A.M., Ruller, R., Prade, R., et al., 2010. Cloning, expression, purification, crystallization and preliminary X-ray diffraction studies of the catalytic domain of a hyperthermostable endo-1,4-beta-D-mannanase from *Thermotoga petrophila* RKU-1. Acta Crystallogr., Sect. F: Struct. Biol. Cryst. Commun. 66, 1078–1081.
Santos, C.R., Squina, F.M., Navarro, A.M., Oldiges, D.P., Leme, A.F., et al., 2011. Functional and biophysical characterization of a hyperthermostable GH51 a-L-arabinofuranosidase from *Thermotoga petrophila*. Biotechnol. Lett. 33, 131–137.
Schneider, T.R., Sheldrick, G.M., 2002. Substructure Solution with SHELXD. Acta Crystallogr., Sect. D: Biol. Crystallogr. 58, 1772–1779.
Schröder, R., Atkinson, R.G., Redgwell, R.J., 2009. Re-interpreting the role of endo-beta-mannanases as mannan endotransglycosylase/hydrolases in the plant cell wall. Ann. Bot. 104, 197–204.
Sheldrick, G.M., 2002. Macromolecular phasing with SHELXE. Z. Kristallogr. 217, 644–650.
Squina, F.M., Santos, C.R., Ribeiro, D.A., Cota, J., Oliveira, R.R., et al., 2010. Substrate cleavage pattern, biophysical characterization and low-resolution structure of a novel hyperthermostable arabinanase from *Thermotoga petrophila*. Biochem. Biophys. Res. Commun. 399, 505–511.
Stålbrand, H., Siika-aho, M., Viikari, L., 1993. Purification and characterization of two β-mannanases from *Trichoderma reesei*. J. Biotechnol. 29, 229–242.
Tailford, L.E., Ducros, V.M., Flint, J.E., Roberts, S.M., Morland, C., et al., 2009. Understanding how diverse beta-mannanases recognize heterogeneous substrates. Biochemistry 48, 7009–7018.
Tanaka, M., Umemoto, Y., Okamura, H., Nakano, D., Tamaru, Y., et al., 2009. Cloning and characterization of a beta-1,4-mannanase 5C possessing a family 27 carbohydrate-binding module from a marine bacterium, *Vibrio* sp. strain MA-138. Biosci. Biotechnol. Biochem. 73, 109–116.
Takahata, Y., Nishijima, M., Hoaki, T., Maruyama, T., 2001. *Thermotoga petrophila* sp. nov. and *Thermotoga naphthophila* sp. nov., two hyperthermophilic bacteria from the Kubiki oil reservoir in Niigata, Japan. Int. J. Syst. Evol. Microbiol. 51, 1901–1909.
Tenkanen, M., Makkonen, M., Perttula, M., Viikari, L., Teleman, A., 1997. Action of *Trichoderma reesei* mannanase on galactoglucomannan in pine kraft pulp. J. Biotechnol. 57, 191–204.
Vagin, A., Teplyakov, A., 1997. MOLREP: an automated program for molecular replacement. J. Appl. Crystallogr. 30, 1022–1025.